**Bartonella henselae Persistence within Mesenchymal Stromal Cells Enhances Endothelial Cell Activation and Infectibility That Amplifies the Angiogenic Process (*Scutera S and Mitola S co-first authors; Sozzani S and Musso T co-last authors)**

(Article begins on next page)

14 December 2021

1  **TITLE**

2  *Bartonella henselae* **Persistence within Mesenchymal Stromal Cells Enhances Endothelial Cells**

3  **Activation and Infectability Amplifying the Angiogenic Process.**

4

5  **Scutera Sara[1]\* Mitola Stefania[2]\* Sparti Rosaria[1] Salvi Valentina[2] Grillo Elisabetta[2] Piersigilli**

6  **Giorgia[1] Bugatti Mattia[2] Alotto Daniela[3] Schioppa Tiziana[2, 4] Sozzani Silvano[5]\* Musso**

7  **Tiziana[1#\*]**

8  [*] Contributed equally

9  [#] Corresponding author

10 **Affiliations**

11 [1]Department of Public Health and Pediatric Sciences, University of Torino, Italy.

12 [2]Department of Molecular and Translational Medicine, University of Brescia, Italy.

13 [3]Skin Bank, Department of General and Specialized Surgery, A.O.U. Città della Salute e della

14 Scienza, Turin, Italy.

15 [4]Humanitas Clinical and Research Center-IRCCS Rozzano-Milano, Italy.

16 [5]Laboratory Affiliated to Istituto Pasteur Italia-Fondazione Cenci Bolognetti, Department of

17 Molecular Medicine, Sapienza University of Rome, Italy.

18 **Correspondence**

19 Tiziana Musso tiziana.musso@unito.it

20

21

22

23

24

25

26

**ABSTRACT**

Some bacterial pathogens can manipulate the angiogenic response, suppressing or inducing it for their own ends. In humans, *B. henselae* is associated with cat-scratch disease and vasculoproliferative disorders such as bacillary angiomatosis and bacillary peliosis. Although endothelial cells (ECs) support the pathogenesis of *Bartonella*, the mechanisms by which *Bartonella* induces EC activation are not completely clear, as well as the possible contribution of other cells recruited at the site of infection. Mesenchymal stromal cells (MSCs) are endowed with angiogenic potential and play a dual role in infections exerting antimicrobial properties but also acting as a shelter for pathogens.

Here we delved into the role of MSCs as reservoir of *Bartonella* and modulator of EC functions. *B. henselae* readily infected MSCs and survived in perinuclear bound vacuoles for up to 8 days. Infection enhanced MSC proliferation and the expression of EGFR, TLR2 and NOD1, proteins that are involved in bacterial internalization and cytokine production. Secretome analysis revealed that infected MSCs secreted higher levels of the proangiogenic factors VEGF, FGF-7, MMP-9, PIGF, serpin E1, TSP-1, uPA, IL-6, PDGF-D, CCL5 and CXCL8. Supernatants from *B. henselae*-infected MSCs increased the susceptibility of ECs to *B. henselae* infection and enhanced EC proliferation, invasion and reorganization in tube-like structures.

Altogether, these results candidate MSCs as a still underestimated niche for *B. henselae* persistent infection and reveal a MSC-EC crosstalk that may contribute to exacerbate bacterial-induced angiogenesis and granuloma formation.

## INTRODUCTION

Endemic among domestic cats, *B. henselae* is a fastidious gram-negative bacterium that, in humans, can cause subclinical intraerythrocytic bacteremia, mainly transmitted by cat fleas. In immunocompetent individuals, *B. henselae* infection can also lead to cat-scratch disease (CSD), characterized by lymphadenopathy with suppurative granulomas. Atypical clinical presentations of CSD, ranging from prolonged fever of unknown origin to hepatosplenic, ocular and neurological manifestations, have also been reported (1).

Individuals unable to mount an immune response against *B. henselae* tend to develop a tumor-like vascular proliferative response in the skin and/or internal organs, which can lead to bacillary angiomatosis (BA) or bacillary peliosis (BP) (2). After infection, *B. henselae* survives, stimulates the migration and the production of pro-angiogenic factors by human endothelial cells (ECs) (2–5). In addition, other cells types, such as monocytes/macrophages (6), recruited to the vasoproliferative lesions, stimulate EC proliferation in a paracrine manner through the production of VEGF and CXCL8 (7). Mononuclear phagocytes, CD34$^+$ progenitor cells and ECs can also function as a reservoir from which *B. henselae* periodically enters the bloodstream and disseminates within the host (8). Despite the clinical implications of protracted *Bartonella* infections, the underlying mechanism of intracellular *B. henselae* persistence is poorly understood, and the existence of different reservoirs still remains to be determined.

Mesenchymal stem cells (MSCs) are multipotent adult stem cells present in various tissues, including the bone marrow and the adipose tissue, which have recently received much attention due to their regenerative potential and immunomodulatory properties (9). MSCs actively participate in angiogenesis through several mechanisms, including paracrine cytokines and exosomes and cell contact interactions with endothelial cells. (10, 11). A diverse and multitasking role of MSCs during bacterial infection has recently emerged (12, 13). MSCs can sense pathogens and mount an appropriate cytokine/chemokine response through the activation of Toll-like receptors (TLRs), NOD-like receptors (NLRs) and the scavenger receptors MARCO and SR-B1 (12). Moreover, MSCs

express EGFR, a (member of the ErbB receptor tyrosine kinase family), shown to enhance their proliferation and the release of angiogenic factors (14).  However, despite the emerging role of MSCs in infectious diseases, the mechanisms regulating the interplay between MSCs and bacteria are yet to be defined. Recent evidence suggests that MSCs can have a double edge sword effect by playing a role in clearing infection but also promoting persistent bacterial infection. MSCs exert antimicrobial effects by secreting antimicrobial peptides and expressing indoleamine2,3-dioxygenase (IDO) and MSC administration reduce pathogen burden in animal models of antimicrobial sepsis (12). However, MSCs  can also serve as a niche where *M. tuberculosis* can survive and persist during antimicrobial therapy. Indeed, viable *M. tuberculosis* was recovered from MSCs infiltrating TB granulomas in humans and in a tuberculosis mouse model (15, 16). It is likely that other chronic bacterial pathogens may exploit MSCs to favor their survival in the host.and  we hypothesized that *B.henselae* infects MSCs and that infected-MSCs contribute to the angiogenesis via interaction with endothelial cells that are one of *Bartonella* preferential target.

Here we show that *B. henselae* can invade and survive within human MSCs and demonstrate that TLR2, NOD1 and EGFR are implicated in bacterial recognition and cytokine production. Moreover, we provides evidence for a MSCs-ECs cross-talk involved in bacteria intracellular survival and activation of a pro-angiogenic program.



**RESULTS**

*B. henselae* **invades and persists in MSCs**. To characterize the interaction of MSCs with *B. henselae,* adipose-derived MSCs were infected with MOI of 100:1 for 1, 2, 3, 4 and 8 days and then treated with gentamicin to kill all residual extracellular bacteria. Subsequently, the number of viable intracellular bacteria was measured by colony-forming unit (CFU) assay. The number of *B. henselae* invading MSCs increased progressively over a 3-day period and the number of CFUs in MSCs

4

104    remained unchanged up to 8 days ($P < 0.05$) (Fig. 1a). At day 8 post-infection (pi), the vast majority

105    of MSCs contained *B. henselae*, as demonstrated by the strong cytoplasmic reactivity of an anti-*B.*

106    *henselae* monoclonal antibody (anti-BH) (Fig. 1b, upper panel). The presence of internalized bacteria

107    was confirmed by immunofluorescence (Fig. 1B, lower panel).      To      assess      *B.      henselae*

108    intracellular survival after the initial infection and gentamicin treatment, MSCs were cultured in

109    medium without gentamicin for four additional days. The number of viable intracellular bacteria

110    recovered, which remained stable during the first 96 h, was significantly lower at day 8 compared to

111    day 4 (Fig. 1c). The ability of *B. henselae* to invade MSCs was further assessed by comparing its

112    infection efficiency in MSCs *vs* HUVECs, a known target of *B. henselae* infection. The number of

113    intracellular bacteria recovered after 24 h of infection from MSCs was significantly higher than that

114    recovered from HUVECs (Fig. 1d).

115        Next, we followed MSC infection by fluorescence microscopy. At day 1 pi, *B. henselae*—

116    stained with DAPI (Cyan)—remained mainly anchored to the MSC membrane, with only a few

117    bacteria present in the cytoplasm (Fig. 2a, upper right panel, arrowhead). From day 2 pi onward, the

118    number of internalized bacteria increased, and most of *B. henselae* were enclosed in perinuclear

119    vesicles   (Fig. 2a, lower left and central panel, thin arrows). After 8 days pi, aggregates of bacteria

120    colocalized with F-actin in globular structures called invasomes, first described in *Bartonella*-infected

121    ECs (Fig. 2a, lower right panel, large arrow; and Fig. 2b) as attested by 3D immunofluorescence

122    analysis.

123        Altogether, these findings indicate that *B. henselae* is internalized by MSCs—even more

124    efficiently than HUVECs—where it can persist for a prolonged time.

125        **B. henselae infection enhances MSC proliferation.** We next asked whether *B. henselae*

126    infection would affect MSC survival. *B. henselae* infection did not induce cell death in MSCs as

127    demonstrated by similar amounts of Annexin V positive cells found in uninfected *vs* infected MSCs

128    (Fig. 3a). This finding was further supported by the unaltered *Bcl-2* (antiapoptotic) /*Bax* (apoptotic)

129  expression ratio observed in these cells (Fig. 3b). We then assessed the effect of infection on the

130  proliferation rate of MSCs. Infected-MSCs grew significantly faster compared to their uninfected

131  counterparts. Conversely, heat-inactivated *B. henselae* (HK *B.henselae*) failed to enhance MSC

132  proliferation (Fig. 3c).

133  **Role of TLR2, EGFR and NOD1 in MSC infection with *B. henselae*.** TLRs and NODs

134  play a key role in bacterial detection and their cooperation become relevant in the context of

135  infections. Interaction between cell surface TLR2 and intracellular surveillance NOD1/2 are of

136  relevance in the recognition of pathogens and in the induction of the inflammatory response (17).

137  However a number of cell surface receptors, such EGFR, that signal through pathways not related to

138  TLRs and NODs, are also used by pathogens and an interaction between TLRs and EGFR has been

139  demonstrated (18, 19).

140  We therefore assessed the expression of these receptors in response to *B. henselae* infection.

141  Interestingly, *B. henselae* infection led to a more than 6-fold increase in TLR2 expression at both

142  mRNA and protein levels, while TLR4 expression remained basically unchanged (Fig. 4a and 4b).

143  Furthermore, RT-PCR analysis showed a significant upregulation of NOD1 mRNA at day 2 and 4 pi

144  (Fig. 4a). NOD2 gene expression was not detected in uninfected or infected MSCs. Lastly, *B.*

145  *henselae* infection significantly increased EGFR mRNA and phosphorylation levels (Fig. 4a and 4c,

146  respectively). Specifically, we detected increased phosphorylation as early as 30 min pi, which

147  remained above basal levels up to 120 min pi (Figure 4c).

148  The involvement of these receptors was evaluated in the production of CXCL8, a cytokine

149  shown to be triggered by *Bartonella* in different cell types (20), *Bartonella* infection of MSCs

150  enhanced their ability to produce CXCL8, which was neutralized by incubation with an anti-TLR2

151  neutralizing antibody (Fig. 4d, upper panel). Similarly, treatment with the EGFR inhibitor gefitinib

152  or with the selective RIP2K inhibitor GSK583 significantly reduced the release of CXCL8 in *B.*

153  *henselae*-infected MSCs (Fig. 4d, lower panel), suggesting that the EGFR/NOD pathway may play a

154  role in CXCL8 transcriptional regulation. Finally, to address the role of bacterium-activated EGFR

155 in *Bartonella* entry, we treated MSCs with the EGFR inhibitor gefitinib and a neutralizing anti-EGFR

156 antibody, detecting a reduced bacterial internalization by about 70% and 50%, respectively, compared

157 to untreated cells (Fig. 4e).

158        **_B. henselae_-infected MSCs promote angiogenesis and infection of endothelial cells.** Since

159 MSCs regulate vascular remodeling and angiogenesis (21), we assessed the pro-angiogenic activity

160 of conditioned medium (CM) from *B. henselae*-infected MSCs. To this end, CM from uninfected or

161 *B. henselae*-infected MSC cultures were tested in a scratch wound healing assay using HUVECs. CM

162 from *B. henselae*-infected MSCs (CM-MSC *B. henselae*), induced a more rapid repair of HUVECs

163 monolayer (Fig. 5a). In addition, the CM-MSC *B. henselae* was 9 fold more powerful then CM of

164 uninfected MCS (CM-MSC CTRL) on aspheroid-based sprouting assay, which faithfully recapitulate

165 the proliferation, invasion and reorganization in tube-like structure of ECs  (Fig. 5b). In keeping with

166 the pro-angiogenic activity of MSCs, the CM-MSC CTRL induced the formation of radial sprouts,

167 similarly to what induced by spheroids stimulation with 30 ng/mL of VEGF-A (Fig. 5b, right panel).

168 Importantly, CM-MSC *B. henselae* but not that from uninfected cells (CM-MSC CTRL) accelerated

169 the morphogenesis of HUVECs when seeded on Cultrex Extracellular Matrix, as judged by the

170 number of closed structures formed at 18 h pi (Fig. 5c).

171        Even though ECs and MSCs can crosstalk through soluble mediators (22), there is no data on

172 the effects of MSC on the susceptibility of ECs to bacterial infection. We thus assessed the extent of

173 *Bartonella* internalization, at day 1 pi, in HUVECs pretreated with CM from uninfected MSCs (CM-

174 MSC CTRL) or *B. henselae*-infected MSCs (CM-MSC *B. henselae*).  While there were no differences

175 in the yield of bacteria between control HUVECs (Ctrl) and HUVECs pretreated with CM-MSC

176 CTRL, a significantly higher number of bacteria was detected in HUVECs pretreated with CM-MSC

177 *B. henselae* (Fig. 5d). After 1 day of culture we did not observe a significant increase in the

178 proliferation of infected HUVECs pre-treated with CM-MSC *B. henselae* over that pre-treated with

179 CM-MSC CTRL, or directly infected. The number of cells harvested/number of cells seeded (mean

180 ± SEM) obtained were 1.23±0.2 (unconditioned medium), 1.063±0.06 (*B. henselae* infected),

7

181  1.125±0.1 (CM-MSC CTRL) and 1.25±0.05 (CM-MSC *B. henselae*). In accord with our observation

182  endothelial cell proliferation during *B. henselae* infection has been shown after 3 or 4 days of

183  incubation (7, 23) . Our results indicate that the treatment with CM-MSC *B. henselae* makes HUVECs

184  more infectable and the increase in intracellular CFU does not depend on HUVEC proliferation.

185  **Angiogenic expression profile of *B. henselae*-infected MSCs.** Finally, we assessed the

186  impact of *B. henselae* infection on the ability of MSCs to modulate the expression of pro-

187  inflammatory and pro-angiogenetic molecules. For this purpose, we probed an antibody angiogenesis

188  array with CM from uninfected and 4-day-infected MSCs. Among the 55 proteins of the assay, 27

189  were detected in CM of both uninfected and infected MSCs. Densitometric analysis showed the

190  upregulation of FGF-7, CXCL8, MMP-9, PIGF, Serpin E1, TSP-1, uPA and VEGF, in *B. henselae*-

191  infected MSCs CM compared to those from uninfected MSCs (Fig. 6a and 6b). Intriguingly, activin

192  A was the only growth factor downregulated in *B. henselae*-infected MSCs (Fig. 6a and 6b). Of note,

193  the elevated expression of MCP-1, PTX3 and TIMP-1 was not modulated by infection (Fig. 6a, and

194  6b). The quantification by ELISA of the increased production of CXCL8 and VEGF in the

195  supernatants of MSCs infected for 1, 4 and 7 days was in good agreement with the array data (Fig.

196  6c). Finally, other molecular factors known for their angiogenic activity, but not included in our array,

197  such as IL-6, CCL5 and PDGF-D, were also induced following *B. henselae* infection (Fig. 6c).

198  **DISCUSSION**

199  *Bartonella* spp exploits several mechanisms to hide inside erythrocytes and ECs to evade

200  immune responses and persist in both animal reservoir and human host. Numerous evidence indicate

201  that the blood-stage phase is preceded by the infection of cellular niches that periodically release

202  bacteria able to invade erythrocytes. ECs were the first cell types considered a primary niche as they

203  support *Bartonella* replication and reside in proximity to the bloodstream (2, 24). However, later

204  studies identified additional *Bartonella* persistence sites including hematopoietic progenitor cells and

205  dendritic cells (8, 25).

206  Here we show that once inside, *B. henselae* resides in MSCs without proliferating for several

8

days. During this time, *Bartonella* localizes in numerous perinuclear membrane bound vacuoles, as previously shown in HUVECs and MonoMac cells (26, 27), or at late time points of infection, as aggregated bacteria enclosed into F actin-rich cell membrane protrusions identified as invasome structures (28).

MSCs sense microorganisms trough the expression of various PRR including Toll-like receptors (TLRs) and Nod-like receptors (NLRs). The engagement of such receptors modulate MSC functions and their abilities to secrete cytokines (29). Our studies revealed that TLR2, NOD1 and EGFR are involved in the recognition and responses to *Bartonella* by MSCs. Upon infection with *B. henselae*, MSCs secret large amounts of CXCL8, which is curbed by incubation with an anti-TLR2 antibody. A central role of TLR2 signaling during *Bartonella* infection is consistent with previous findings indicating that *B. henselae*, despite being Gram-negative, preferentially activates TLR2 (25). In infected cells, NOD1 and NOD2 recognize bacterial peptidoglycan derivatives released into the cytosol and, upon ligand association with the adaptor protein receptor-interacting-serine/threonine-protein kinase 2 (RIPK2 or RIP2), trigger proinflammatory signaling (30). In our experimental system, inhibition of the RIP2 with the highly RIPK2-specific compound GSK583(31) decreased CXCL8 release, indicating that NOD1 activation and signaling through RIP2 during MSC infection is, in part, responsible for inducing the inflammatory response to *B. henselae* infection. Consistent with our results, NOD1 mediates CXCL8 induction after recognition of *Helicobacter pylori*, *Escherichia coli* (32, 33) and *Chlamydia pneumoniae* (34). Importantly, gefitinib, an inhibitor of EGFR tyrosine kinase domain, used to treat various forms of cancer, can hamper *B. henselae*-mediated induction of CXCL8, suggesting a role of EGFR in this pathway. Gefitinib also exerts an off-target inhibitory activity on the expression of RIP2 (35), thus the inhibition of CXCL8 secretion may be due to blockage of NOD/RIP2 signaling alongside that of EGFR. In support to this hypothesis, EGFR/NOD cooperation has been recently involved in cytokine production in dengue virus infected monocytes (36). Moreover, a growing body of literature highlights the importance of EGFR/ErbB in several bacterial and viral inflammatory responses (18, 37) and in pathogenic angiogenesis (38). In

9

233  addition to stimulation of EGFR tyrosine phosphorylation, *Bartonella* enhanced EGFR mRNA

234  expression suggesting that this upregulation could serve as a positive feedback system. A functional

235  role of EGFR signaling in the immune response against *B. henselae* is further supported by the

236  observation that treatment of MSCs with the kinase inhibitor gefitinib or an anti-EGFR antibody

237  significantly decreases *Bartonella* internalization. In this regard, EGFR has been recently shown to

238  act as a cofactor in mediating pathogen internalization in host cells (e.g., HBV, HCV, Chlamydia and

239  Candida) (18). Our finding indicates an important role of EGFR activation in *Bartonella* invasion;

240  however, as these EGFR inhibitors do not completely abrogate *Bartonella* uptake by MSCs, it is

241  likely that other receptors, other than EGFR, may play a role in *Bartonella* infection. Moreover, it

242  remains to be investigated whether EGFR activation is due to the direct interaction of *Bartonella* with

243  the EGFR extracellular domain or by its transactivation by EGFR ligands (i.e., EGF, HBEGF, TGFα,

244  BTC, AREG, EREG and EPGN) as shown for *H. pylori* and *Neisseria* spp. (39, 40). EGFR signaling

245  pathways exert an antiapoptotic activity in *Pseudomonas-* and *Helicobacter-* infected cells (41, 42)

246  suggesting that EGFR activation by *Bartonella* promotes the survival and proliferation of infected

247  MSCs.

248      These effects may also be explained at least in part by the robust release of cytokine/growth

249  factors caused by *Bartonella* infection.  In addition to CXCL8, angiogenic factors upregulated in

250  infected MSCs include FGF-7, MMP-9, PIGF, serpin E1, TSP-1, uPA, IL-6, CCL5 and VEGF,

251  leading to the induction of a pro-angiogenic phenotype in ECs as well as an increased susceptibility

252  of ECs to infection.. Data reporting a role of MSCs in facilitating the infection of other cell types are

253  sparse and concern mainly phagocytic cells. MSCs was shown to enhance bacterial uptake and

254  clearance by PMNs (43), and to mediate the reactivation of HIV in monocytic cells (44). A secretome

255  highly rich in inflammatory angiogenic cytokines and matrix remodeling factors was previously

256  described in *B. henselae* infected myeloid angiogenic cells (MACs). Similarly to our observation in

257  MSCs conditioned  medium from MACs increased angiogenic sprouting (45). In the past, infected

258  ECs have been shown to upregulate the expression of VEGF and CXCL-8 that  directly lead to host

10

259  cell proliferation and potentiate angiogenesis (23, 46); in parallel, *Bartonella* triggers the release of

260  proinflammatory chemokines which recruit monocytes/macrophages in the vasoproliferative lesions

261  and the production of angiogenic factors by phagocytic cells upon infection plays a central role in

262  mediating angiogenesis-(7, 20, 45). . Since at sites of infection/inflammation, MSCs localize in

263  contact with ECs (22, 47), we propose that infected MSCs may support this angiogenic loop.

264      A role for MSCs can be envisioned in different scenarios of *Bartonella* infections. For

265  instance, MSCs are recruited in tuberculosis around the lymph node granulomas to establish a

266  persistent infection and likely to suppress T cell response (48). Moreover, MSCs are found in oral

267  pyogenic granuloma tissues (49). Granulomatous lymphadenitis is the pathological hallmark of cat

268  scratch disease whereby MSCs could also be hired in *Bartonella* granuloma to contribute to the

269  immune pathogenesis. MSCs reside in the bone marrow (BM) interacting with other cellular

270  components. We have previously shown the co-localization DCs and MSCs in human BM (50). The

271  role of MSC-EC crosstalk has been characterized in the maintenance of the hematopoietic stem cell

272  niche and in infection-induced emergency myelopoiesis (51, 52). Interestingly MSCs were shown to

273  regulate proliferation and erythroid differentiation of $CD34^+$ stem cells (53). As *B. henselae* can infect

274  $CD34^+$ BM progenitor cells, BM has been proposed as one of the potential niches. In this regard,

275  multifocal BM involvement was shown in CSD (54, 55) and a contribution of *B. henselae* to

276  ineffective erythropoiesis was suggested (56). *Bartonella*-infected MSCs, releasing soluble

277  molecules, can recruit and activate ECs which in turn collaborate with MSCs in the fine regulation of

278  the hematopoietic stem cell niche.

279      In conclusion, this study provides novel insights into the role of MSCs in serving as a reservoir

280  during *B. henselae* infection and identifies TLR2, NOD1 and EGFR as the receptors involved in the

281  recognition of *B. henselae*. Infection of MSCs triggers a potent proangiogenic program, which

282  activates and enhances EC susceptibility to bacterial infection. A better understanding of the

283  involvement of MSCs in *Bartonella*-induced angiogenesis may allow the development of targeted

284  therapeutic strategies for the treatment of vascular proliferative disorders.

## MATERIALS AND METHODS

**Cell culture.** Human MSCs were isolated from adipose tissues as previously described (50). Human adipose tissues were collected by lipoaspiration from healthy donors after written consent and in compliance with the Declaration of Helsinki and the local Ethic Committee (Comitato Etico Interaziendale A.O.U. Città della Salute e della Scienza di Torino - A.O. Ordine Mauriziano - ASL TO1, No. 0009806). Subsequently, MSCs were analyzed by flow cytometry to verify their phenotype was positive for CD73, CD90 and CD105 and negative for CD11b, CD34 and CD45.

HUVECs were isolated from umbilical cords of healthy informed volunteers in compliance with the Declaration of Helsinki. HUVECs were used at early (I-IV) passages and grown on culture plates coated with porcine gelatin in M199 medium (Gibco Life Technologies, ThermoFisher Scientific Group) supplemented with 20% heat-inactivated fetal calf serum (FCS, Gibco Life Technologies), endothelial cell growth factor (ECGF) (10 µg/mL), and porcine heparin (100 µg/mL) (Sigma Aldrich) (100 µg/mL) or in complete EBM2 medium (Lonza Group Ltd Basel, Switzerland).

**Bacterial cultures.** *B. henselae* Houston I strain (ATCC 49882; Manassas, VA, USA) was grown on 5% sheep blood Columbia agar plates (BioMerieux, Lyon, France) under anaerobic conditions (i.e., candle jar) at 37°C for 10 days. Bacteria were harvested under a laminar-flow hood by gently scraping colonies off the agar surface. They were then suspended in MICROBANK™ cryopreservative solution and stored at -80°C in 1-mL aliquots. For biological assays, frozen bacteria were incubated in Schneider's Insect Medium (Sigma-Aldrich) supplemented with 10% FBS, as described by Riess et al (57), at 37°C and 5% $CO_2$ for 6 days. Spectrophotometry was performed to evaluate bacterial growth [optical density (OD600) 0.6, corresponding to $1x10^8$ bacteria/mL] and confirmed by plating serial dilutions on 5% sheep blood Columbia agar plates. Bacteria, washed 3 times with 1X PBS, were then added to cell cultures. Where indicated, *B. henselae* were killed by heating thawed bacteria at 56°C for 30 min.

**Preparation of conditioned medium.** MSCs, cultured into 12-well plates at a density of

12

311    $0.5 \times 10^5$ cells/well in RPMI 10% FBS without antibiotics, were left untreated or infected for 96 h

312    with *B. henselae*. Cells were then extensively washed to remove extracellular bacteria, and fresh

313    RPMI was replaced for 72 h. Conditioned medium was collected, centrifuged at 4000 rpmi for 10

314    min and then filtered, aliquoted, and stored at -20°C.

315        **Infection assay.** *B. henselae* invasion of MSCs was assessed by GPA. Briefly, 12,500

316    cells/cm² MSCs were seeded for 24 h in RPMI supplemented with 10% FCS. To compare MSCs with

317    HUVECs, infection was carried out with 60,000 cells *per* well seeded in DMEM 10% FCS or

318    complete EBM2 medium (Lonza Group Ltd), respectively. The next day, cells were washed twice

319    and cultured in RPMI supplemented with 10% FCS without antibiotics. *B. henselae* (MOI 100) was

320    added to the cells, immediately centrifuged at 1200 g for 5 min to allow the association of bacteria

321    with the cellular surface, and incubated for 1, 2, 3, 4 and 8 days. At the end of infection period,

322    gentamicin sulfate (Sigma-Aldrich) (100 µg/mL) was added to the medium for 2 h to kill all

323    extracellular bacteria—this assay was performed in triplicate, and control wells were left uninfected.

324    Cells were then washed extensively and lysed by the addition of 200 µL of distilled water for 5 min

325    and sonicated for 1.30 min. Lysates were serially diluted, plated on Columbia blood agar, and CFUs

326    were counted after 1 week of incubation. To determine intracellular survival after 96 h of infection,

327    extracellular bacteria were killed by gentamicin treatment for 2 h. Cells were further incubated in

328    normal medium for the remaining time of the indicated infection period. When indicated, cells were

329    pretreated for 6 h with the specific inhibitors gefitinib (10 µM) and GSK583 (1 µM) (both from

330    MedChemExpress NJ, USA) or with a specific antibody against EGFR (mouse IgG1, clone LA1) or

331    its corresponding isotype control antibody (both from EMD Millipore Corporation CA, USA) at 10

332    µg/ml.. GPA was performed as described above after 1 or 2 days. In some experiments, HUVECs

333    were cultured in the presence of CM from untreated and infected MSCs. Briefly cells seeded at 60,000

334    cells per well were pretreated overnight with the indicated CM and then infected with *B. henselae*

335    (MOI 100) for 24 h. Cells were harvested and counted directly with an hemacytometer. Proliferation

336    is reported as an index calculated as number of cells harvested/number of cells seeded. In parallel a

337    GPA assay was performed.

338         **Staining procedures.** MSCs ($1 \times 10^4$) were seeded on glass coverslips and infected with *B.*

339    *henselae* at a MOI of 100. For immunohistochemical staining, cells were fixed in methanol, saturated

340    with 0.1% BSA in PBS and incubated for 1h with an anti-*B henselae* mAb (anti-BH, dilution 1:50,

341    mouse IgG2b/clone H2A10,  Abcam , Cambridge, United Kingdom).The H2A10 clone reacts with a

342    43-kDa epitope present only in *B. henselae* strains and not in other Bartonella species (58). After

343    washing an anti-mouse biotinylated Ab was added for 30 min. and the slides were then stained with

344    horseradish peroxidase streptavidin (HRP Streptavidin) or with the chromogen DAB (3, 3'-

345    diaminobenzidine) (ThermoFisher Scientific). For immunofluorescence analysis, the slides were

346    incubated with anti-BH mAb, followed by goat anti-mouse Alexa Fluor® 594 (dilution 1:500,

347    A21023, ThermoFisher Scientific). Nuclei were counterstained with DAPI (4',6-diamidin-2-

348    fenilindolo) (ThermoFisher Scientific). To follow bacterial infection, MSCs were seeded at $0.25 \times 10^4$

349    on glass coverslips, infected with *B. henselae* (MOI 100) and incubated for 1, 2, 3, 4 and 8 days. At

350    the end of infection period, cells were fixed with 4% paraformaldehyde (PFA) for 10', washed with

351    PBS and permeabilized in PBS with 0.25% saponin. Samples were then saturated with blocking

352    solution (PBS with 5% normal goat serum, and 2% BSA) for 1h at RT. After washes in PBS, samples

353    were incubated with the wheat germ agglutinin-Alexa Fluor 594 or 488 conjugate, Alexa Fluor® 594

354    phalloidin (A12381) (1 h) and with DAPI (5 min) (all from ThermoFisher Scientific CA, USA) to

355    stain cell membranes, actin and nuclei/bacteria respectively.  Cells were analyzed under a Zeiss

356    Observer.Z1 epifluorescence microscope equipped with a Plan-Apochromat 100×/1.4 NA oil

357    objective and ApoTome2 imaging system for optical sectioning. Z-stack images were elaborated

358    through AxioVision 3D and Extended Focus modules.

359         **Immunoblotting**. Total cell lysates from cellsuntreated or treated for 30, 60 and 120 min.

360    with *B. henselae* (MOI 100) or with 50 ng/ml EGF (R&D System, MN, USA) for 15 min, were

361    prepared in cold lysis buffer (1% Triton X-100, 1% NP-40 in PBS, pH 7.4) containing a cocktail of

362    protease and phosphatase inhibitors (Sigma-Aldrich). Samples (10-20 μg) were analyzed by 10%

SDS-PAGE under denaturing conditions, followed by Western blotting, using the antibodies against EGFR (clone A10, sc-373746), pY1068-EGFR (sc-377547) and secondary antibodies HRP-conjugated (all from Santa Cruz Biotechnology, Inc.,Texas, USA). ~~the indicated antibodies~~ . Chemiluminescent signal (Clarity Western ECL Substrate, Bio-Rad) was acquired by ChemiDoc$^{TM}$ Imaging System (BioRad).

**Real-time PCR**. Total MSC RNA isolated with the Qiagen RNeasy mini kit was treated with DNase I (Qiagen, Hilden, Germany) and retrotranscribed into cDNA by iScript cDNA Synthesis Kit (Bio-Rad Laboratories Inc., Hercules, CA, USA). Gene specific primers were: TLR-2 (sense, 5'- CTCATTGTGCCCATTGCTCTT -3'; antisense, 5'- TCCAGTGCTTCAACCCACAAC -3'), TLR-4 (sense, 5'- GGCCATTGCTGCCAACAT -3'; antisense, 5'- CAACAATCACCTTTCGGCTTTT -3'), Bax (sense, 5'- AGAGGATGATTGCCGCCGT -3'; antisense, 5'- CAACCACCCTGGTCTTGGATC -3'), Bcl-2 (sense, 5'- TGCA.CCTGACGCCCTTCAC -3'; antisense, 5'- AGACAGCCAGGAGAAATCAAACAG -3'), HPRT (sense, 5'- TGACCTTGATTTATTTTGCATACC -3'; antisense, 5'- CGCTTTCCATGTGTGAGGTGATG -3'), RPL13A (sense, 5'-CATAGGAAGCTGGGAGCAAG-3'; antisense, 5'- GCCCTCCAATCAGTCTTCTG-3'). For EGFR, NOD1 and NOD2, validated primers from Bio-Rad were used (Unique Assay ID qHsaCID0007564, qHsaCED0005079 and qHsaCED0056944 respectively). For quantitative real-time PCR, the iQTM SYBR Green Supermix (Bio-Rad Laboratories Inc., Segrate, MI, Italy) was used according to the manufacturer's instructions. Reactions were run in duplicate on a CFX96 Real Time System and analyzed by BioRad CFX Maestro Software (Bio-Rad Laboratories Inc.). Gene expression was normalized to HPRT or RPL13A mRNA content.

**MTT assay.** MSC cell viability was measured by MTT 3-(4,5-dimethylthiazol-2-yl)-2,5-diphenyltetrazolium bromide assay (Sigma Aldrich, MO, USA). Cells were seeded at a density of $2x10^3$/well in 96-well plates. After 24 h of incubation in RPMI 10% FBS without antibiotics, cells

were infected with *B. henselae* (MOI 100). The medium was changed after 4 days to wash out all extracellular bacteria. When indicated, cells were treated with heat-killed *B. henselae*. Cells were then incubated for 3 h with 20 µl MTT (final concentration 0,5 mg/ml). Formazan crystals were solubilized for 10 min in 100 µl DMSO, and OD 570 nm was measured using a microplate reader (VICTOR3™, PerkinElmer, MA, USA). To determine the contribution of bacteria in MTT reduction to overall values of infected MSCs, a bacterial suspension with the same concentrations per milliliter of those recovered from cells was assessed in parallel and the obtained values subtracted to results from infected cells. **Annexin V Assay.** MSCs untreated or infected for 96 h with *B. henselae* were stained with annexin V-FITC and PI (Sigma Aldrich) according to the manufacturer's instructions. Samples were analyzed by FACS Calibur (Becton Dickinson), and results were quantified using FlowLogic (Miltenyi Biotec, Bergisch Gladbach, Germany).

**Flow cytometry.** MSCs were collected at the indicated times after infection and preincubated for 30 min at 4°C in 1X PBS supplemented with 2% goat serum and 0.2% sodium azide, washed twice with 1% bovine serum albumin (BSA). Successively, cells were incubated for 30 min at 4°C with anti-human TLR-2 FITC (mouse IgG2a) and anti-human TLR-4 PE (mouse IgG2a) or respective isotype controls (all from BioLegend CA, USA). Flow cytometry analysis was performed using FACS Calibur and FlowLogic as described above.

**Cytokine measurements.** MSCs seeded in 24-well plates were infected with a MOI of 100 for the indicated times. For some experiments, cells werepretreated with the pharmacological inhibitors gefitinib and GSK583 or the ~~neutralizing antibody anti-TLR2 ).~~ The neutralizing antibody anti-TLR2 (anti-human TLR2-IgA, clone B4H2) and the human IgA2 isotype control (both purchased from InvivoGen, CA, USA). Cell-free supernatants were then harvested to measure human VEGF-A, CXCL8, IL-6 and CCL5 production by ELISA (R&D Systems, Minneapolis, MN, USA). To quantify human PDGF-D, a specific kit from Elabscience (Wuhan, Hubei, P.R.C) was employed.

**Angiogenesis array.** The human angiogenesis array (Proteome Profiler™ Array; R&D

Systems) was used to assess the expression of 55 angiogenic-related proteins in MSCs uninfected or infected with *B. henselae* for 96 h. The array membranes were probed with pooled supernatants derived from three independent experiments according to manufacturer's instructions. Chemiluminescent signal was acquired by ChemiDoc™ Imaging System (BioRad).

The signal intensity of each antigen-specific antibody spot was quantified using Fiji-ImageJ (NIH) software. For comparison of the relative expression of proteins in uninfected *vs* infected cells, the mean pixel density of the pair of duplicate spots for each protein, after subtraction of the mean pixel density of the negative control spots of the respective array, was normalized to the mean pixel density of the positive control spots. Heat map analysis using the normalized data was performed by GraphPad PRISM 8.0 software.

**Sprouting assay.** Sprouting of HUVEC spheroids was assessed as described previously (59). Briefly, spheroids were prepared in 20% methylcellulose medium, embedded in a fibrin gel and stimulated with recombinant human VEGF-A$_{165}$ (30 ng/mL) (R&D System, MN, USA) or with different concentrations of CM from uninfected or infected MSCs. The number of radially growing cell sprouts was counted after 24 h using an Axiovert 200M microscope equipped with LD A Plan 20X/0.30PH1 objective (Carl Zeiss) and expressed as relative increase over untreated spheroids.

**Motility assay**. HUVEC motility assay was based on "scratch" wounding of a confluent monolayer. Briefly, HUVECs ($1 \times 10^5$) were seeded onto 0.1 % collagen type I (BD Biosciences, Italy)-coated six-well plates in complete medium until a confluent monolayer was formed. The cell monolayers were scratched using a pipette tip, washed with 1X PBS to remove the undetached cells and treated with MSC conditioned medium. After 24 h, cells were photographed under an Axiovert 200M microscope (Carl Zeiss) equipped with LD A Plan 20X/0.30PH1. The healed area was quantified through computerized analysis by subtracting the wound area at 24 h from the initial area.

**Tube formation assay.** EC vessel formation was assessed by tube morphogenesis assay in a three-dimensional (3D) collagen matrix. To this end, HUVECs were seeded onto Reduced Growth

440 Factor Basement Membrane Matrix Cultrex® (BME) (Trevigen, Italy)-coated μ-slide angiogenesis

441 chamber (Ibidi, Martinsried, Germany) at a density of $4.0 \times 10^4$ cells/cm$^2$ in the absence or presence

442 of CM from untreated or infected MSCs. After 48 h, cells were photographed using an Axiovert 200M

443 microscope, and the number of meshes/field was counted. **Statistical    Analysis.**    Statistical

444 significance was determined by non-parametric Student's t-test and one-way analysis of variance

445 followed by Tukey's multiple-comparison test. Results were analyzed by GraphPad PRISM 8.0

446 software (CA, USA).

447

448 **Abbreviations**

449 MSCs: mesenchymal stromal cells

450 ECs: endothelial cells

451 DCs: dendritic cells

452 TLRs: Toll-like receptors

453 NLRs:  NOD-like receptors

454 PRRs: Pattern Recognition Receptors

455 CSD: cat scratch disease

456 BA: bacillary angiomatosis

457  BP: bacillary peliosis

458 GPA: gentamicin protection assay

459 CM: conditioned medium

460 MOI: multiplicity of infection

461 BM: bone marrow

462 ANOVA: analysis of variance

463

464 **Acknowledgments**

18

466      University of Brescia, for immunohistochemistry analysis of the MSC/*B. henselae* interaction.

467

468      **DECLARATIONS**

469      **Funding**

473      **Conflict of Interest Statement**

474      The authors declare that the research was conducted in the absence of any commercial or financial

475      relationships that could be construed as a potential conflict of interest.

476      **Ethics Statement**

477      This study was carried out in accordance with the recommendations of "Comitato Etico

478      Interaziendale A.O.U. Città della Salute e della Scienza di Torino—A.O. Ordine Mauriziano—ASL

479      TO1, number 0009806" with written informed consent from all subjects. All subjects gave written

480      informed consent in accordance with the Declaration of Helsinki. The protocol was approved by the

481      "Comitato Etico Interaziendale A.O.U. Città della Salute e della Scienza di Torino—A.O. Ordine

482      Mauriziano—ASL TO1."

483      **Availability of data and materials**

484      All data and materials are available upon request.

485      **Author Contributions**

486      SaS, SM, SiS, and TM participated in the design of the study.

487      SaS, RS, GP, EG, MB, VS, DA, and TS participated in data acquisition and analysis.

488      TM, SM and SaS wrote the manuscript.

489      SiS participated in data interpretation and manuscript revision.

490

491

492

**REFERENCES**

493

494    1.    Florin TA, Zaoutis TE, Zaoutis LB. 2008. Beyond Cat Scratch Disease: Widening Spectrum of Bartonella

495          henselae Infection. Pediatrics 121:e1413–e1425.

496    2.    Harms A, Dehio C. 2012. Intruders below the Radar: Molecular Pathogenesis of Bartonella spp. Clin

497          Microbiol Rev 25:42–78.

498    3.    McCord AM, Burgess AWO, Whaley MJ, Anderson BE. 2005. Interaction of Bartonella henselae with

499          Endothelial Cells Promotes Monocyte/Macrophage Chemoattractant Protein 1 Gene Expression and

500          Protein Production and Triggers Monocyte Migration. Infect Immun 73:5735–5742.

501    4.    Berrich M, Kieda C, Grillon C, Monteil M, Lamerant N, Gavard J, Boulouis HJ, Haddad N. 2011.

502          Differential Effects of Bartonella henselae on Human and Feline Macro- and Micro-Vascular

503          Endothelial Cells. PLoS ONE 6:e20204.

504    5.    Tsukamoto K, Shinzawa N, Kawai A, Suzuki M, Kidoya H, Takakura N, Yamaguchi H, Kameyama T,

505          Inagaki H, Kurahashi H, Horiguchi Y, Doi Y. 2020. The Bartonella autotransporter BafA activates the

506          host VEGF pathway to drive angiogenesis. Nat Commun 11:3571.

507    6.    Musso T, Badolato R, Ravarino D, Stornello S, Panzanelli P, Merlino C, Savoia D, Cavallo R, Ponzi AN,

508          Zucca M. 2001. Interaction of Bartonella henselae with the Murine Macrophage Cell Line J774:

509          Infection and Proinflammatory Response. Infect Immun 69:5974–5980.

510    7.    Resto-Ruiz SI, Schmiederer M, Sweger D, Newton C, Klein TW, Friedman H, Anderson BE. 2002.

511          Induction of a Potential Paracrine Angiogenic Loop between Human THP-1 Macrophages and Human

512          Microvascular Endothelial Cells during Bartonella henselae Infection. Infect Immun 70:4564–4570.

513    8.    Mändle T, Einsele H, Schaller M, Neumann D, Vogel W, Autenrieth IB, Kempf VAJ. 2005. Infection of

514          human CD34+ progenitor cells with Bartonella henselae results in intraerythrocytic presence of B

515          henselae. Blood 106:1215–1222.

516    9.    Pittenger MF, Discher DE, Péault BM, Phinney DG, Hare JM, Caplan AI. 2019. Mesenchymal stem cell

517          perspective: cell biology to clinical progress. Npj Regen Med 4:22.

518    10.   Melchiorri AJ, Nguyen B-NB, Fisher JP. 2014. Mesenchymal Stem Cells: Roles and Relationships in

519          Vascularization. Tissue Eng Part B Rev 20:218–228.

520    11.   Di Somma M, Schaafsma W, Grillo E, Vliora M, Dakou E, Corsini M, Ravelli C, Ronca R, Sakellariou P,

521          Vanparijs J, Castro B, Mitola S. 2019. Natural Histogel-Based Bio-Scaffolds for Sustaining Angiogenesis

522          in Beige Adipose Tissue. Cells 8:1457.

523    12.   Alcayaga-Miranda F, Cuenca J, Khoury M. 2017. Antimicrobial Activity of Mesenchymal Stem Cells:

524          Current Status and New Perspectives of Antimicrobial Peptide-Based Therapies. Front Immunol 8.

525    13.   Bessède E, Dubus P, Mégraud F, Varon C. 2015. Helicobacter pylori infection and stem cells at the

526          origin of gastric cancer. 20. Oncogene 34:2547–2555.

527    14.   De Luca A, Gallo M, Aldinucci D, Ribatti D, Lamura L, D'Alessio A, De Filippi R, Pinto A, Normanno N.

528          2011. Role of the EGFR ligand/receptor system in the secretion of angiogenic factors in mesenchymal

529          stem cells. J Cell Physiol 226:2131–2138.

530    15.   Das B, Kashino SS, Pulu I, Kalita D, Swami V, Yeger H, Felsher DW, Campos-Neto A. 2013. CD271+ Bone

531          Marrow Mesenchymal Stem Cells May Provide a Niche for Dormant Mycobacterium tuberculosis. Sci

532          Transl Med 5:170ra13-170ra13.

533    16.   Fatima S, Kamble SS, Dwivedi VP, Bhattacharya D, Kumar S, Ranganathan A, Van Kaer L, Mohanty S,

534          Das G. 2019. Mycobacterium tuberculosis programs mesenchymal stem cells to establish dormancy

535          and persistence. J Clin Invest 130:655–661.

536     17.    Oviedo-Boyso J, Bravo-Patiño A, Baizabal-Aguirre VM. 2014. Collaborative Action of Toll-Like and Nod-

537            Like Receptors as Modulators of the Inflammatory Response to Pathogenic Bacteria. Mediators

538            Inflamm 2014:1–16.

539     18.    Ho J, Moyes DL, Tavassoli M, Naglik JR. 2017. The Role of ErbB Receptors in Infection. Trends

540            Microbiol 25:942–952.

541     19.    Koff JL, Shao MXG, Ueki IF, Nadel JA. 2008. Multiple TLRs activate EGFR via a signaling cascade to

542            produce innate immune responses in airway epithelium. Am J Physiol-Lung Cell Mol Physiol

543            294:L1068–L1075.

544     20.    McCord AM, Resto-Ruiz SI, Anderson BE. 2006. Autocrine Role for Interleukin-8 in Bartonella

545            henselae-Induced Angiogenesis. Infect Immun 74:5185–5190.

546     21.    Rezaie J, Heidarzadeh M, Hassanpour M, Amini H, Shokrollahi E, Ahmadi M, Rahbarghazi R. 2020. The

547            Angiogenic Paracrine Potential of Mesenchymal Stem Cells, p. . *In* Ahmed Al-Anazi, K (ed.), Update on

548            Mesenchymal and Induced Pluripotent Stem Cells. IntechOpen.

549     22.    Nassiri SM, Rahbarghazi R. 2013. Interactions of Mesenchymal Stem Cells with Endothelial Cells. Stem

550            Cells Dev 23:319–332.

551     23.    Kempf VA, Volkmann B, Schaller M, Sander CA, Alitalo K, Riess T, Autenrieth IB. 2001. Evidence of a

552            leading role for VEGF in Bartonella henselae-induced endothelial cell proliferations. Cell Microbiol

553            3:623–632.

554     24.    Dehio C. 2005. Bartonella –host-cell interactions and vascular tumour formation. 8. Nat Rev Microbiol

555            3:621–631.

556     25.    Vermi W. 2006. Role of dendritic cell-derived CXCL13 in the pathogenesis of Bartonella henselae B-

557            rich granuloma. Blood 107:454–462.

558    26.    Kempf VAJ, Schaller M, Behrendt S, Volkmann B, Aepfelbacher M, Cakman I, Autenrieth IB. 2000.

559           Interaction of Bartonella henselae with endothelial cells results in rapid bacterial rRNA synthesis and

560           replication. Cell Microbiol 2:431–441.

561    27.    Kempf VAJ, Schairer A, Neumann D, Grassl GA, Lauber K, Lebiedziejewski M, Schaller M, Kyme P,

562           Wesselborg S, Autenrieth IB. 2005. Bartonella henselae inhibits apoptosis in Mono Mac 6 cells: B.

563           henselae inhibits apoptosis in monocytes. Cell Microbiol 7:91–104.

564    28.    Truttmann MC, Misselwitz B, Huser S, Hardt W-D, Critchley DR, Dehio C. 2011. Bartonella henselae

565           engages inside-out and outside-in signaling by integrin β1 and talin1 during invasome-mediated

566           bacterial uptake. J Cell Sci 124:3591–3602.

567    29.    Najar M, Krayem M, Meuleman N, Bron D, Lagneaux L. 2017. Mesenchymal Stromal Cells and Toll-Like

568           Receptor Priming: A Critical Review. Immune Netw 17:89.

569    30.    Strober W, Murray PJ, Kitani A, Watanabe T. 2006. Signalling pathways and molecular interactions of

570           NOD1 and NOD2. Nat Rev Immunol 6:9–20.

571    31.    Haile PA, Votta BJ, Marquis RW, Bury MJ, Mehlmann JF, Singhaus R, Charnley AK, Lakdawala AS,

572           Convery MA, Lipshutz DB, Desai BM, Swift B, Capriotti CA, Berger SB, Mahajan MK, Reilly MA, Rivera

573           EJ, Sun HH, Nagilla R, Beal AM, Finger JN, Cook MN, King BW, Ouellette MT, Totoritis RD,

574           Pierdomenico M, Negroni A, Stronati L, Cucchiara S, Ziółkowski B, Vossenkämper A, MacDonald TT,

575           Gough PJ, Bertin J, Casillas LN. 2016. The Identification and Pharmacological Characterization of 6-(

576           *tert* -Butylsulfonyl)- *N* -(5-fluoro-1 *H* -indazol-3-yl)quinolin-4-amine (GSK583), a Highly Potent and

577           Selective Inhibitor of RIP2 Kinase. J Med Chem 59:4867–4880.

578    32.    Viala J, Chaput C, Boneca IG, Cardona A, Girardin SE, Moran AP, Athman R, Mémet S, Huerre MR,

579           Coyle AJ, DiStefano PS, Sansonetti PJ, Labigne A, Bertin J, Philpott DJ, Ferrero RL. 2004. Nod1 responds

580           to peptidoglycan delivered by the Helicobacter pylori cag pathogenicity island. Nat Immunol 5:1166–

581           1174.

23

582    33.    Kim JG, Lee SJ, Kagnoff MF. 2004. Nod1 Is an Essential Signal Transducer in Intestinal Epithelial Cells

583           Infected with Bacteria That Avoid Recognition by Toll-Like Receptors. Infect Immun 72:1487–1495.

584    34.    Opitz B, Förster S, Hocke AC, Maass M, Schmeck B, Hippenstiel S, Suttorp N, Krüll M. 2005. Nod1-

585           Mediated Endothelial Cell Activation by *Chlamydophila pneumoniae*. Circ Res 96:319–326.

586    35.    Tigno-Aranjuez JT, Asara JM, Abbott DW. 2010. Inhibition of RIP2's tyrosine kinase activity limits

587           NOD2-driven cytokine responses. Genes Dev 24:2666–2677.

588    36.    Duran A, Valero N, Mosquera J, Fuenmayor E, Alvarez-Mon M. 2017. Gefitinib and pyrrolidine

589           dithiocarbamate decrease viral replication and cytokine production in dengue virus infected human

590           monocyte cultures. Life Sci 191:180–185.

591    37.    Bentz GL, Yurochko AD. 2008. Human CMV infection of endothelial cells induces an angiogenic

592           response through viral binding to EGF receptor and β1 and β3 integrins. Proc Natl Acad Sci 105:5531–

593           5536.

594    38.    Singh B, Carpenter G, Coffey RJ. 2016. EGF receptor ligands: recent advances. F1000Research 5:2270.

595    39.    Swanson KV, Griffiss JM, Edwards VL, Stein DC, Song W. 2011. Neisseria gonorrhoeae-induced

596           transactivation of EGFR enhances gonococcal invasion. Cell Microbiol 13:1078–1090.

597    40.    Keates S, Keates AC, Katchar K, Peek, Jr. RM, Kelly CP. 2007. *Helicobacter pylori* Induces Up-Regulation

598           of the Epidermal Growth Factor Receptor in AGS Gastric Epithelial Cells. J Infect Dis 196:95–103.

599    41.    Zhang J, Li H, Wang J, Dong Z, Mian S, Yu F-SX. 2004. Role of EGFR Transactivation in Preventing

600           Apoptosis in Pseudomonas aeruginosa–Infected Human Corneal Epithelial Cells. Invest Ophthalmol

601           Vis Sci 45:2569–2576.

602    42. Yan F, Cao H, Chaturvedi R, Krishna U, Hobbs SS, Dempsey PJ, Peek RM, Cover TL, Washington MK,

603         Wilson KT, Polk DB. 2009. Epidermal growth factor receptor activation protects gastric epithelial cells

604         from Helicobacter pylori-induced apoptosis. Gastroenterology 136:1297–1307, e1-3.

605    43. Brandau S, Jakob M, Bruderek K, Bootz F, Giebel B, Radtke S, Mauel K, Jäger M, Flohé SB, Lang S. 2014.

606         Mesenchymal Stem Cells Augment the Anti-Bacterial Activity of Neutrophil Granulocytes. PLOS ONE

607         9:e106903.

608    44. Chandra PK, Gerlach SL, Wu C, Khurana N, Swientoniewski LT, Abdel-Mageed AB, Li J, Braun SE,

609         Mondal D. 2018. Mesenchymal stem cells are attracted to latent HIV-1-infected cells and enable virus

610         reactivation via a non-canonical PI3K-NFκB signaling pathway. Sci Rep 8:14702.

611    45. O'Rourke F, Mändle T, Urbich C, Dimmeler S, Michaelis UR, Brandes RP, Flötenmeyer M, Döring C,

612         Hansmann M-L, Lauber K, Ballhorn W, Kempf VAJ. 2015. Reprogramming of myeloid angiogenic cells

613         by Bartonella henselae leads to microenvironmental regulation of pathological angiogenesis. Cell

614         Microbiol 17:1447–1463.

615    46. Kempf VAJ, Hitziger N, Riess T, Autenrieth IB. 2002. Do plant and human pathogens have a common

616         pathogenicity strategy? Trends Microbiol 10:269–275.

617    47. Del Prete A, Scutera S, Sozzani S, Musso T. 2019. Role of osteopontin in dendritic cell shaping of

618         immune responses. Cytokine Growth Factor Rev 50:19–28.

619    48. Raghuvanshi S, Sharma P, Singh S, Van Kaer L, Das G. 2010. Mycobacterium tuberculosis evades host

620         immunity by recruiting mesenchymal stem cells. Proc Natl Acad Sci 107:21653–21658.

621    49. Dehghani Nazhvani A, Ahzan S, Hosseini S-M, Attar A, Monabati A, Tavangar MS. 2018. Purification of

622         Stem Cells from Oral Pyogenic Granuloma Tissue. Open Dent J 12:560–566.

25

623    50.    Scutera S, Salvi V, Lorenzi L, Piersigilli G, Lonardi S, Alotto D, Casarin S, Castagnoli C, Dander E,

624           D'Amico G, Sozzani S, Musso T. 2018. Adaptive Regulation of Osteopontin Production by Dendritic

625           Cells Through the Bidirectional Interaction With Mesenchymal Stromal Cells. Front Immunol 9:1207.

626    51.    Mitroulis I, Kalafati L, Bornhäuser M, Hajishengallis G, Chavakis T. 2020. Regulation of the Bone

627           Marrow Niche by Inflammation. Front Immunol 11.

628    52.    Tamma R, Ribatti D. 2017. Bone Niches, Hematopoietic Stem Cells, and Vessel Formation. Int J Mol Sci

629           18.

630    53.    Perucca S, Di Palma A, Piccaluga PP, Gemelli C, Zoratti E, Bassi G, Giacopuzzi E, Lojacono A, Borsani G,

631           Tagliafico E, Scupoli MT, Bernardi S, Zanaglio C, Cattina F, Cancelli V, Malagola M, Krampera M, Marini

632           M, Almici C, Ferrari S, Russo D. 2017. Mesenchymal stromal cells (MSCs) induce ex vivo proliferation

633           and erythroid commitment of cord blood haematopoietic stem cells (CB-CD34+ cells). PloS One

634           12:e0172430.

635    54.    Hipp SJ, O??Shields A, Fordham LA, Blatt J, Hamrick HJ, Henderson FW. 2005. Multifocal Bone Marrow

636           Involvement in Cat-Scratch Disease: Pediatr Infect Dis J 24:472–474.

637    55.    Donà D, Nai Fovino L, Mozzo E, Cabrelle G, Bordin G, Lundin R, Giaquinto C, Zangardi T, Rampon O.

638           2018. Osteomyelitis in Cat-Scratch Disease: A Never-Ending Dilemma—A Case Report and Literature

639           Review. Case Rep Pediatr 2018:1–8.

640    56.    Randell MG, Balakrishnan N, Gunn-Christie R, Mackin A, Breitschwerdt EB. 2018. Bartonella henselae

641           infection in a dog with recalcitrant ineffective erythropoiesis. Vet Clin Pathol 47:45–50.

642    57.    Riess T, Dietrich F, Schmidt KV, Kaiser PO, Schwarz H, Schäfer A, Kempf VAJ. 2008. Analysis of a Novel

643           Insect Cell Culture Medium-Based Growth Medium for Bartonella Species. Appl Environ Microbiol

644           74:5224–5227.

26

645    58.    Rolain JM, La Scola B, Liang Z, Davoust B, Raoult D. 2001. Immunofluorescent detection of

646         intraerythrocytic Bartonella henselae in naturally infected cats. J Clin Microbiol 39:2978–2980.

647    59.    Rezzola S, Di Somma M, Corsini M, Leali D, Ravelli C, Polli VAB, Grillo E, Presta M, Mitola S. 2019.

648         VEGFR2 activation mediates the pro-angiogenic activity of BMP4. Angiogenesis 22:521–533.

649

650

651

652    **FIGURE LEGENDS**

653

654    **FIG. 1 *B. henselae* invades and persists in MSCs.** (a) Invasion rates of *B. henselae* into MSCs were

655    measured at day 1, 2, 3, 4 and 8 pi by gentamicin protection assay (GPA). After infection, cells were

656    treated with gentamicin, and the number of intracellular bacteria was determined by CFU count. Data

657    are expressed as mean $\pm$ SEM from two independent experiments carried out in triplicate (*$P < 0.05$

658    *vs* $Log_{10}$ CFU at 1 day; unpaired t-test). (b) Uninfected (CTRL) or *B. henselae*-infected MSCs (8

659    days) were immunostained with an anti-*BH* antibody and counterstained with hematoxylin (upper

660    panel 20X, lower panel 40X) or with goat anti-mouse Alexa Fluor® 594 conjugate and DAPI for

661    immunofluorescence visualization (lower panel 100X). (c) To determine intracellular survival after

662    4 days of infection, extracellular bacteria were killed by gentamicin treatment and incubated in normal

663    medium for the indicated times. Mean values $\pm$ SEM of four independent experiments performed in

664    triplicate (*$P < 0.05$; unpaired t-test). (d) Invasion rates of *B. henselae* in MSCs or HUVECs (60,000

665    cells each, respectively). The number of intracellular bacteria as $Log_{10}$ CFU was quantified at 1 day

666    pi. Mean $\pm$ SEM of three experiments (*$P < 0.05$ MSCs *vs* HUVECs; unpaired t-test).

667    **FIG. 2 *B. henselae* localizes in invasome structures in MSCs**. (a) Immunofluorescence of *B.*

668    *henselae*-infected MSCs at 1, 2, 4 and 8 days pi and uninfected control MSCs (CTLR). *B. henselae*

669    and cell membranes were stained with DAPI (cyan) and wheat germ agglutinin-Alexa Fluor 594 (red),

27

respectively, and analyzed with an epifluorescence microscope. Bacteria anchored to the MSC

membrane are indicated with arrowheads. The thin arrows (2 and 4 days) indicate internalized

bacteria within membrane bound compartments in the perinuclear area, whereas the large arrows (8

days) highlight sizeable intracellular bacterial aggregates called invasomes. Each image also shows

the basal portion of adherent MSC cells, with the orthogonal z reconstruction of the whole cell. (b)

Representative image of an invasome. MSCs were infected with *B. henselae* for 8 days and then

washed and fixed with PFA. Samples were stained for F-actin (red), wheat germ agglutinin (WGA)

(green) and DAPI and analyzed as described in panel a (bar: 10 µm).

**FIG. 3 *B. henselae* favors the proliferation of infected MSCs.** (a) MSC death was evaluated by

FACS analysis after 4 days of infection with *B. henselae.* Uninfected MSCs (left panel; CTRL) and

infected MSCs (right panel; *B. henselae*) were double-stained with FITC-annexin V and PI.

Counterstaining with PI allowed differentiation of necrotic cells (upper left quadrant of the dot plot),

late apoptotic cells (upper right quadrant) and early apoptotic cells (lower right quadrant). The

percentages of cells localizing to these quadrants are indicated in each quadrant. Data are

representative of three independent experiments. (b) The Bcl-2/Bax expression ratio was analyzed in

control and *B. henselae*-infected MSCs at 2 days pi by qPCR. Gene expression was normalized to

HPRT. Data are expressed as mean ± SEM of four independent experiments (ns not significant;

unpaired t-test). (c) Proliferation assay. MSCs were treated as indicated for 0, 2, 4, and 8 days and

analyzed by MTT assay. Untreated MSCs (white circle); *B. henselae* infected MSC (black circle);

and heat killed *B. henselae*-treated MSCs (HK *B.henselae*) (grey circle). Data are expressed as mean

± SEM of three independent experiments performed in triplicate(*$P < 0.05$ *B. henselae vs* CTRL,

unpaired t-test).

**FIG. 4 Expression of TLR2, NOD1 and EGFR in *B. henselae*-infected MSCs**. (a) mRNA

expression levels of TLR2, TLR4, NOD1 and EGFR in uninfected (white bar) and *B. henselae*-

infected MSCs (black bar) were determined by qPCR and normalized to RPL13A. Data are expressed

695 as mean ± SEM of four independent experiments (* *P* < 0.05; unpaired t-test). (b) TLR2 and TLR4

696 protein expression levels on MSC membranes were analyzed by FACS in MSCs at 4 days pi. Cells

697 were immunostained with anti-TLR2, anti-TLR4 or specific isotype control antibodies. The

698 percentages of positive cells are indicated in each quadrant. Fluorescence minus one (FMO) controls

699 for the antibodies are shown as well. Data are representative of three independent experiments (left

700 panel) or as mean ± SEM (right panel). (c) Cell extracts from MSCs infected with *B. henselae* for 30,

701 60, and 120 min or with hEGF (50 ng/mL) for 15 min were subjected to immunoblotting using anti-

702 EGFR pY1068 or anti-EGFR antibodies. (d) Analysis of CXCL8 in the supernatants from uninfected

703 or *B. henselae*-infected MSCs pre-treated or not for 6 h with a neutralizing anti-TLR2 antibody (10

704 μg/mL) (upper panel, n=6 experiments) or with the EGFR inhibitor gefitinib (10 μM) or the RIP2K

705 inhibitor GSK583 (1 μM) (lower panel, n= 4 experiments) and then stimulated for 96 h. Data are

706 shown as percentage (means ± SEM) of CXCL8 production compared to specific isotype control

707 antibody or DMSO respectively set as 100% (* *P* < 0.05 *vs B. henselae*-infected cells; unpaired t-

708 test). (e) To evaluate *B. henselae* internalization, MSCs were pretreated for 6 h with the neutralizing

709 anti-EGFR (10 μg/mL) (upper panel, n=3 independent experiments) or gefitinib (10 μM) (lower

710 panel, n=4 independent experiments), and CFU values of intracellular bacteria, determined, after 1

711 and 2 days of incubation, are expressed as percentage relative to CFU of specific isotype control

712 antibody or DMSO-treated cellsset as 100%. Data are shown as mean ± SEM; * *P* < 0.05 *vs*

713 internalized bacteria in untreated cells; unpaired t-test.

714 **FIG. 5 Conditioned medium from *B. henselae*-infected MSCs curbs the infection rates and**

715 **angiogenic response of HUVECs.** The effects of conditioned medium (CM) from *B. henselae*-

716 infected MSCs were tested by means of different angiogenic assays. (a) HUVEC monolayers were

717 wounded with a 1.0-mm-wide rubber policeman and incubated in fresh medium supplemented with

718 5% FCS and 1:2 diluted CM from infected (black bar, CM-MSC CTRL) or uninfected (white bar,

719 CM-MSC *B. henselae*) MSCs. After 1 day, HUVECs invading the wound were quantified by digital

imaging to calculate the relative increment in cell-covered area induced by MSC-CM compared to untreated HUVECs. Mean ± SEM of three independent experiments. *$P < 0.05$ *vs* Ctrl; unpaired t-test. (b) Sprouting analysis of HUVEC spheroids. Spheroids were prepared in 20% methylcellulose medium, embedded in fibrin gel and stimulated with 1:2 diluted CM obtained from MSCs treated in the presence (black bar) or absence (white bar) of bacteria or with 30 ng/ml VEGF-A (dashed bar). The number of growing cell sprouts was counted after 1 day. Data are expressed as mean fold change vs Ctrl ± SEM of 20-40 spheroids/ experimental condition in three independent experiments and indicated as fold increase in the number of sprouts/spheroid *vs* Ctrl. *$P < 0.05$*vs* Ctrl; unpaired t-test. (c) The effect of CM from uninfected *vs B. henselae*-infected MSCs on HUVEC morphogenesis was assessed by tube morphogenesis assay in three-dimensional (3D) collagen matrix. HUVECs were seeded (40000 cells/cm$^2$) on Cultrex Extracellular Matrix in the presence of 1:2 diluted CM from uninfected (white bar) or *B. henselae*-infected MSCs (black bar). After 8 h, the formation of capillary-like structures was examined. Representative images are shown in the left panels. Quantification (right panel) was performed to calculate the relative increment in capillary-like structure induced by MSC-CM compared to untreated HUVECs. Data are expressed as mean ± SEM relative to three independent experiments. * $P < 0.05$ *vs* Ctrl; unpaired t-test. (d) Invasion rate of *B. henselae* in HUVECs (expressed as total CFUs) after 1 day of infection in the absence (grey bar) or presence of 1:2 diluted CM-MSC CTRL (white bar) and CM-MSC *B. henselae* (black bar). Mean ± SEM of three independent experiments * $P < 0.05$; unpaired t-test.

**FIG. 6 Angiogenic signature of *B. henselae*-infected MSCs.** (a) Human angiogenesis antibody array analysis was performed using a pool of supernatants from 96 h uninfected MSC (CTRL) or *B. henselae*-infected MSCs. Some of the most representative angiogenic factors are highlighted in different colors. (b) Representative heat map (left panel) and relative gene expression shown as normalized pixel density of the duplicated spots for each angiogenic-related protein in the array of supernatants of MSCs and *B. henselae*-infected MSCs (right panel). * $P < 0.01$ ** $P < 0.001$ vs CTRL;

745 ANOVA followed by Tukey's multiple-comparison test. (c) Quantification of VEGF-A, CXCL8, IL-

746 6, CCL5 and PDGF-D production in uninfected (CTRL) and *B. henselae*-infected MSCs. Data are

747 expressed as mean ± SEM of three independent experiments. * P < 0.05 *vs* CTRL; unpaired t-test.

748 nd= not detectable.

749

750

751

752

753

754

755

756

757

758
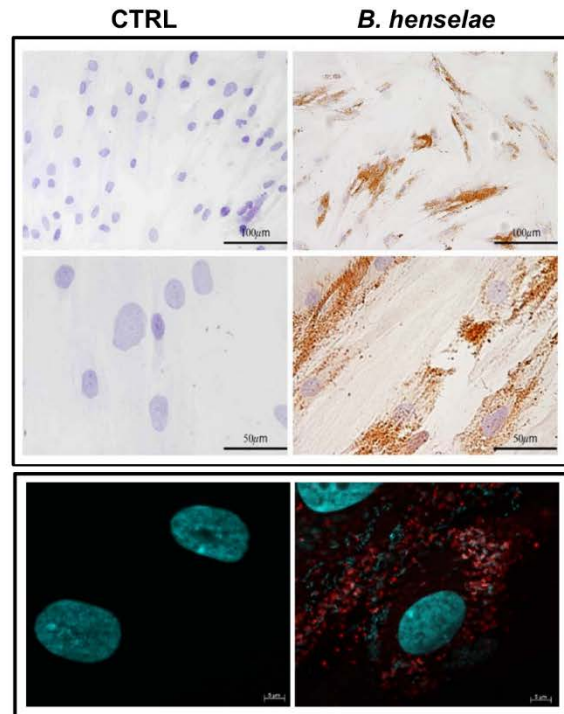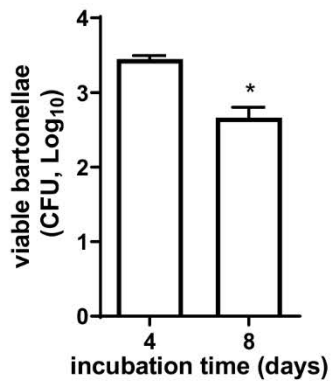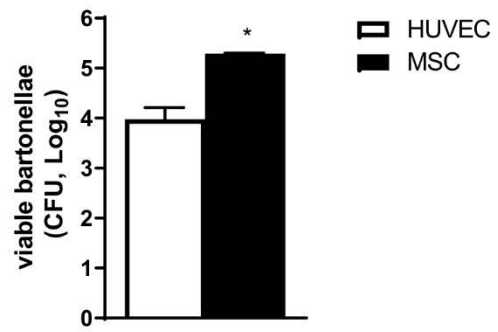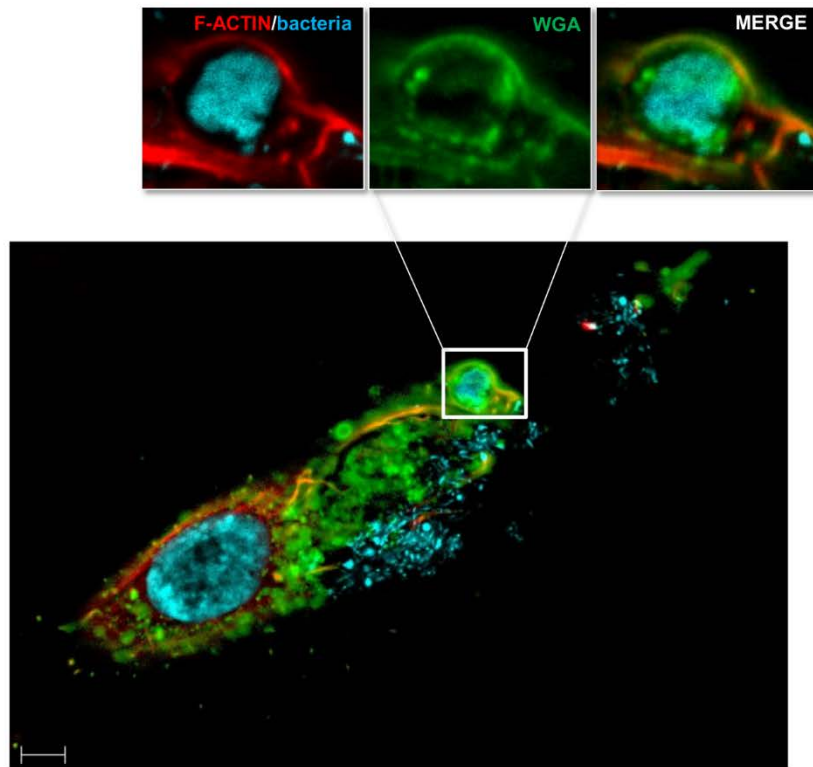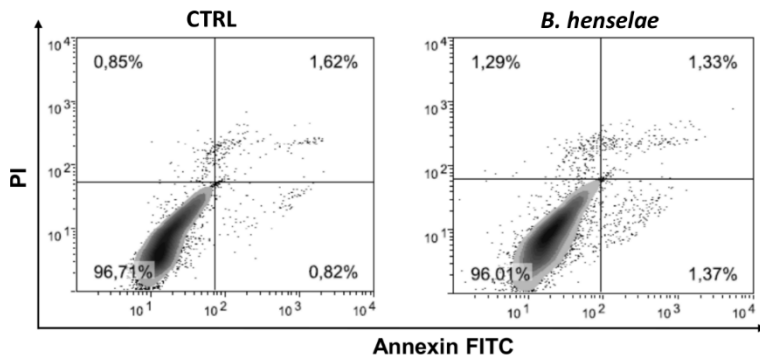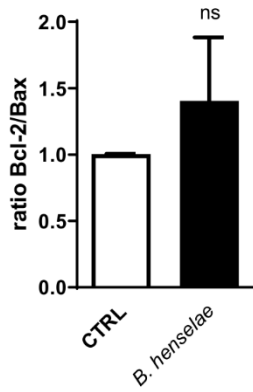
759

760

761

762

763

764
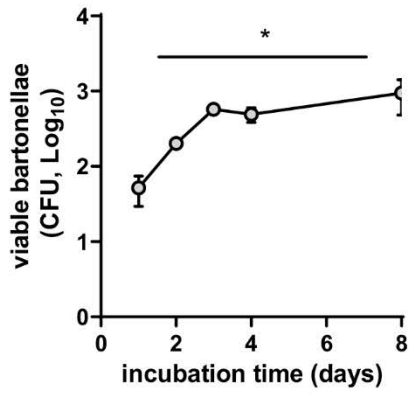
**Figure 1**

767
768
769
770
771
772
773
774
775

776    **Figure 2**

777

778

779
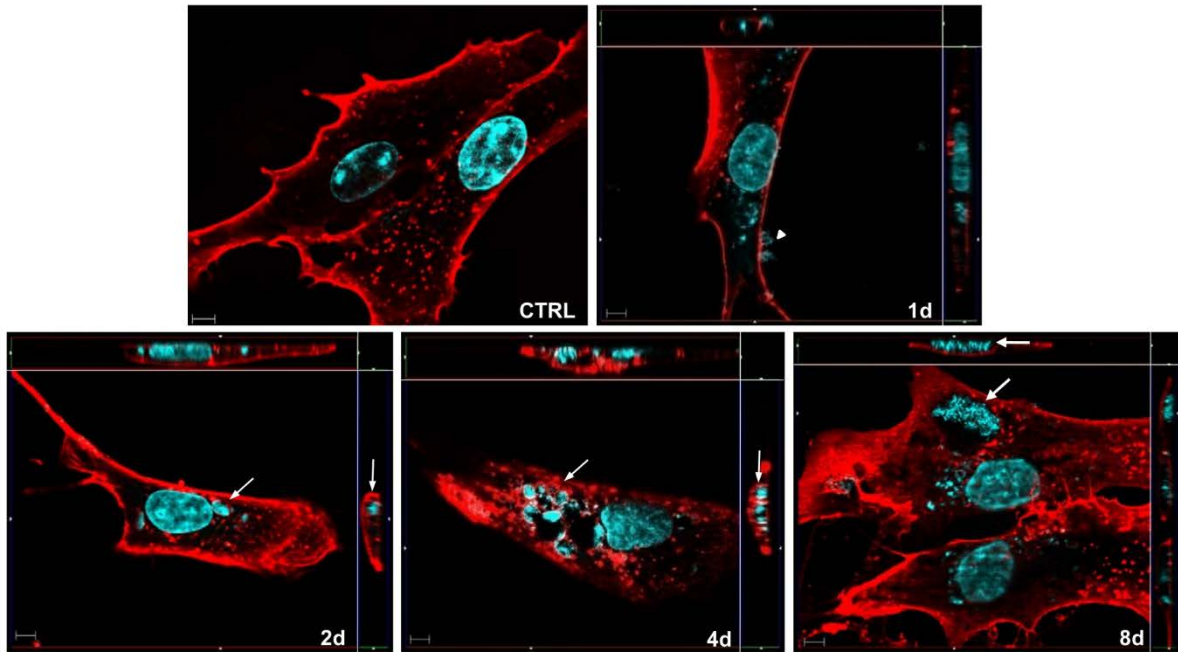
**Figure 3**

**A**



**B**

**C**
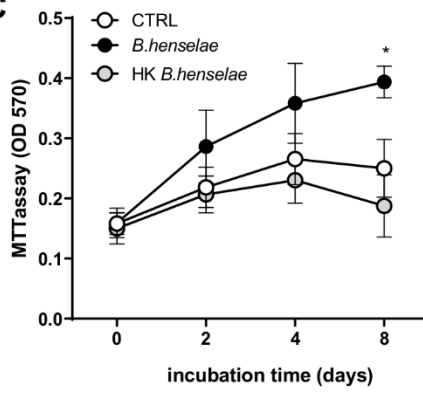
781

782

783

784

785

786

787

788

789

790

791

792

793

794

795

796
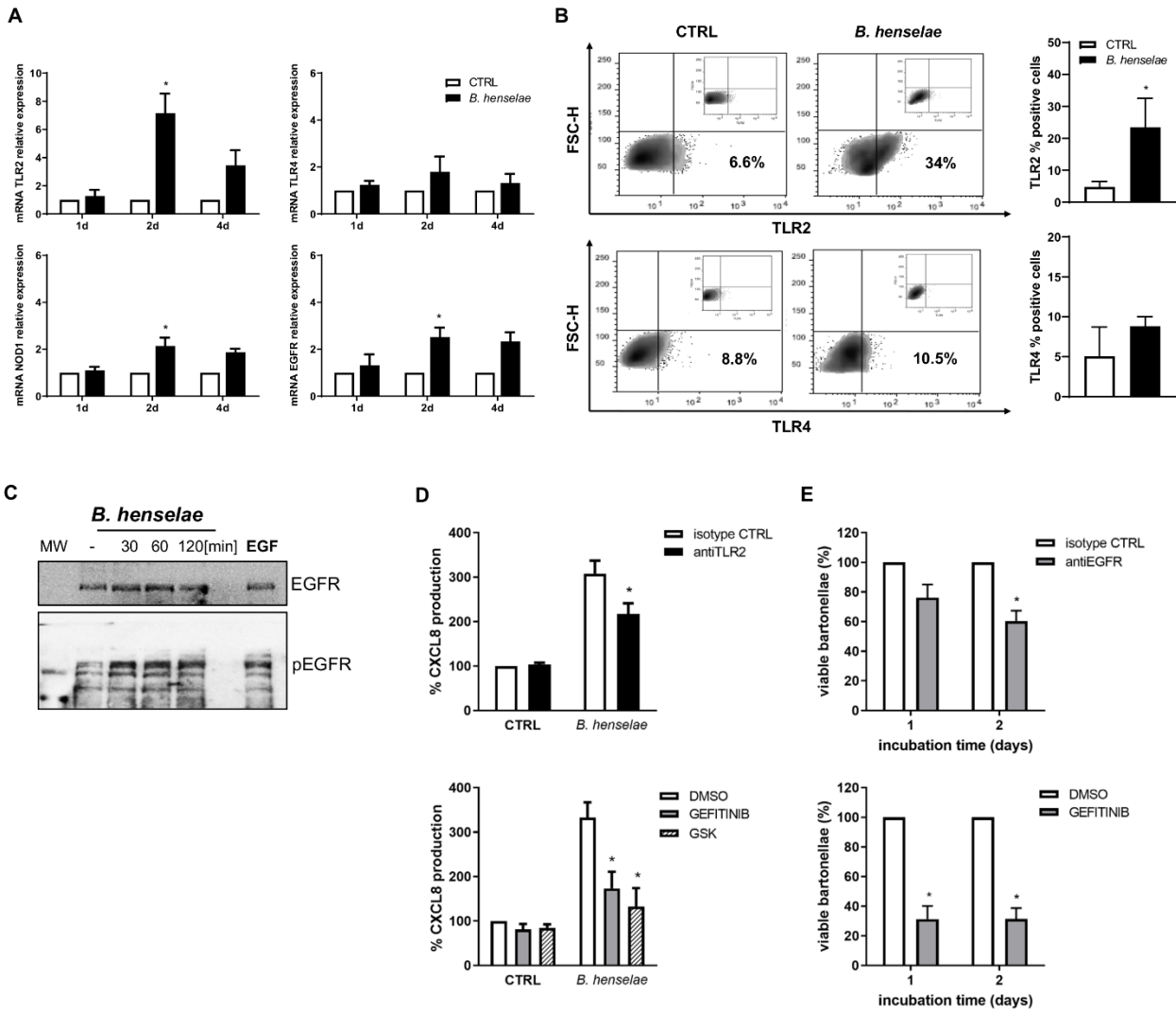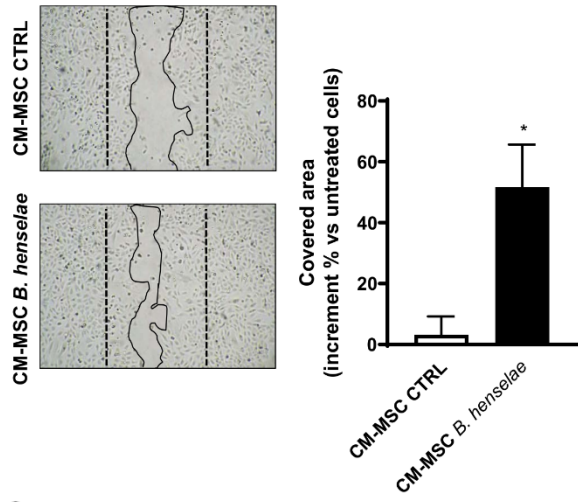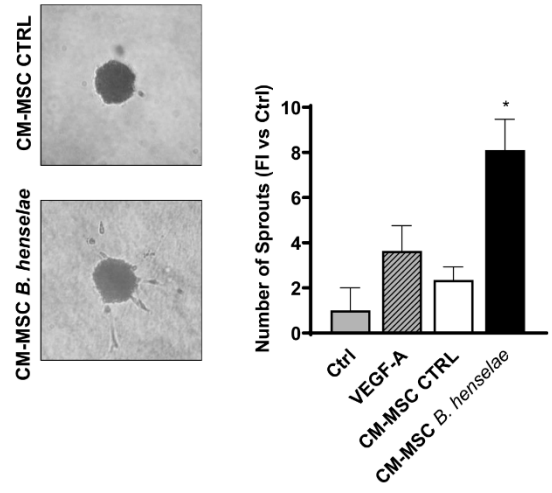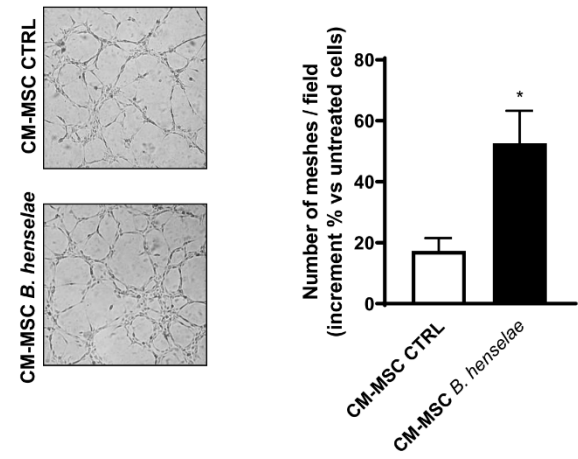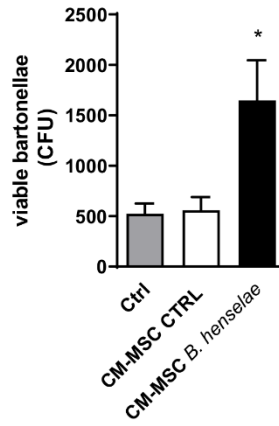
**Figure 4**

**Figure 5**
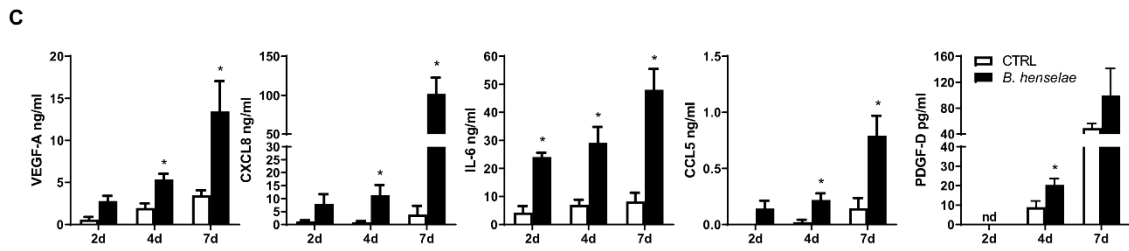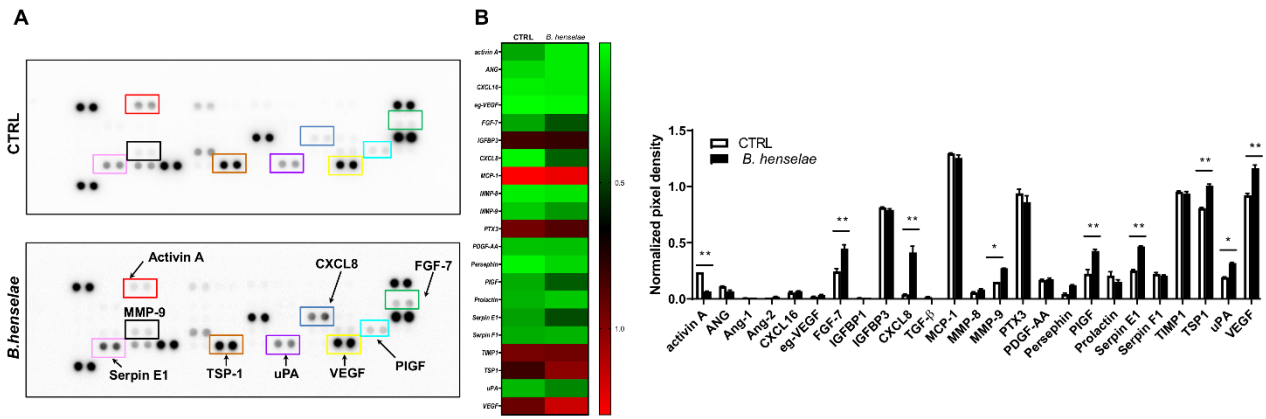
824    **Figure 6**



825
826
827
828
829
830
831
832
833
834
835
836

37